

A Numerical Study of Improved Quark Actions on Anisotropic Lattices¹

Shiquan Su^a, Liuming Liu^a, Xin Li^a and Chuan Liu^a

^a*School of Physics
Peking University
Beijing, 100871, P. R. China*

Abstract

Tadpole improved Wilson quark actions with clover terms on anisotropic lattices are studied numerically. Using asymmetric lattice volumes, the pseudo-scalar meson dispersion relations are measured for 8 lowest lattice momentum modes with quark mass values ranging from the strange to the charm quark with various values of the gauge coupling β and 3 values of the bare speed of light parameter ν . These results can be utilized to extrapolate or interpolate to obtain the optimal value for the bare speed of light parameter ν_{opt} at a given gauge coupling for any given type of meson. In particular, the optimal values of ν for η_c , D and D_s pseudo scalar mesons are given for various gauge couplings. The lattice action with these optimized parameters can then be used to study physical properties of hadrons involving either light or heavy quarks.

Key words: Non-perturbative renormalization, improved actions, anisotropic lattice .

PACS: 12.38Gc, 11.15Ha

1 Introduction

It has become clear that anisotropic lattices and improved lattice actions are the ideal candidates for lattice QCD calculations involving heavy objects like the glueballs, one meson states with non-zero three momenta and multi-meson states with or without three momenta. It is also a good workplace for the

¹ This work is supported by the Key Project of National Natural Science Foundation of China (NSFC) under grant No. 10235040 and supported by the Trans-century fund from Chinese Ministry of Education.

study of hadrons with heavy quarks. In this work we present our numerical study on the quark action parameters suitable for heavy flavor physics. The gauge action employed in this paper is the tadpole improved gluonic action on asymmetric lattices:

$$\begin{aligned}
S = & -\beta \sum_{i>j} \left[\frac{5 \text{Tr} P_{ij}}{9 \xi u_s^4} - \frac{1 \text{Tr} R_{ij}}{36 \xi u_s^6} - \frac{1 \text{Tr} R_{ji}}{36 \xi u_s^6} \right] \\
& -\beta \sum_i \left[\frac{4 \xi \text{Tr} P_{0i}}{9 u_s^2} - \frac{1 \xi \text{Tr} R_{i0}}{36 u_s^4} \right]
\end{aligned} \tag{1}$$

where P_{ij} is the usual plaquette variable and R_{ij} is the 2×1 Wilson loop on the lattice. The parameter u_s , which we take to be the fourth root of the average spatial plaquette value, incorporates the so-called tadpole improvement and ξ designates the (bare) aspect ratio of the anisotropic lattice. With the tadpole improvement in place, the bare anisotropy parameter ξ suffers only small renormalization which we neglect in this study. Using this action, glueball and light hadron spectrum has been studied within the quenched approximation [1,2,3,4,5,6,7].

It has been suggested that relativistic heavy quarks can also be treated with the help of anisotropic lattices (the Fermi lab approach), possibly with improvements [8,9,10,11,12]. Using various versions of the quark actions, charmed meson spectrum, charmonium spectrum, charmed baryons have been studied on the lattice [13,14,15,16,17,18]. Another type of application of the anisotropic lattices is the calculation of hadron-hadron scattering lengths within the quenched approximation [19,20,21,22]. However, in order to take full advantage of the improved quark action on anisotropic lattices, some parameters in the action have to be determined, either perturbatively or non-perturbatively, in order to gain as much improvement as possible. Some numerical studies of these parameters have already appeared in the literature [23,12,24,25,26]. The anisotropic quark actions used in these studies fall into two categories. These two cases differ mainly in the choice of spatial Wilson parameter r_s . According to the tree-level study [8,11], the choice of $r_s = 1/\xi$ has a virtue that the optimal parameters in the action as a function of the quark mass contains no corrections of the form $m_0 a_s$. The quark mass dependent corrections comes in only in terms of $m_0 a_t$ which is assumed to be small. As a result, the optimal values of the parameters can be approximated by their values in the zero quark mass limit. That is to say, tuning of the parameters in the action becomes almost quark mass independent. The disadvantage of this choice is that the doublers are not very well separated from the ordinary fermions, particularly for large ξ . In the other choice, one sets $r_s = 1$. This presumably elevates the doublers well above the ordinary fermion modes, however, the optimal values of the parameters in this choice might receive $O(m_0 a_s)$ corrections, as suggested by tree-level and one-loop perturbative studies [8,11]. Therefore, if one takes the

choice of $r_s = 1$, optimal values of the action parameters in principle must be tuned in a quark *mass-dependent* way.

In this paper, we will discuss the tuning of the bare speed of light parameter ν in a quenched calculation using tadpole-improved Wilson fermions on anisotropic lattices. The parameter ν has to be tuned such that the pseudo-scalar meson energy-momentum dispersion relation reproduces its continuum form in the low-momentum limit. The dispersion relations of pseudo-scalar mesons are measured in our simulation for quark mass values ranging from the strange to the charm quark mass. These results of pseudo-scalar meson dispersion relations at different values of ν then enable us to extrapolate/interpolate to the optimized value of the bare speed of light parameter ν for a particular type of meson at a given gauge coupling β . In order to measure the meson dispersion relations with better accuracy, asymmetric spatial lattice volumes are used which provide us with more non-degenerate (in the sense of energy) low-momentum modes. The quark action thus obtained can then be utilized in future studies on physical properties of hadrons with either light or heavy quarks.

This paper is organized in the following manner. In Section 2, a particular form of clover-improved Wilson fermion action on anisotropic lattices is introduced. In Section 3, the calculation of the dispersion relation for pseudo-scalar meson is discussed. This is performed for quark mass values ranging from the strange all the way to the charm quark mass at various values of gauge coupling and bare speed of light parameter ν . By extrapolation or interpolation, the optimal values of the bare speed of light (denoted by ν_{opt}) can then be determined for various values of β once a particular type of meson is chosen. In particular, we focus on three cases which correspond to the η_c meson, D meson and D_s meson respectively. The optimal values of ν for these three cases are obtained. In Section 4, we will conclude with some general remarks.

2 Improved Wilson Fermions on Anisotropic Lattices

Consider a finite four-dimensional lattice with lattice spacing a_μ along the μ direction with $\mu = 0, 1, 2, 3$. For definiteness, we denote $a_0 = a_t$ and $a_i = a_s$ for $i = 1, 2, 3$. We will use $\xi = a_s/a_t$ to denote the bare aspect ratio of the asymmetric lattice. The quark actions on anisotropic lattices have been studied extensively in the literature [8,9,10,27,14,11,28,23,16,12,25,24,26] Using these actions, charmed meson spectrum [13,17], charmonium spectrum [14,16], charmed baryon spectrum [15,18] and hadron-hadron scattering lengths [19,20,21,22] have been studied.

We start from the fermion action in the hopping parameter parametrization:

$$\begin{aligned}
S &= \bar{\psi}_x M_{xy} \psi_y , \\
M_{xy} &= \left[1 + \kappa_s c_B \sum_{i < j} \sigma_{ij} \mathcal{F}_{ij} + \kappa_s c_E \sum_i \sigma_{0i} \mathcal{F}_{0i} \right] \delta_{xy} \\
&\quad - \kappa_t \left[(1 - \gamma_0) U_0(x) \delta_{x+\hat{0},y} + (1 + \gamma_0) U_0^\dagger(x - \hat{0}) \delta_{x-\hat{0},y} \right] \\
&\quad - \kappa_s \sum_i \left[(1 - \gamma_i) U_i(x) \delta_{x+\hat{i},y} + (1 + \gamma_i) U_i^\dagger(x - \hat{i}) \delta_{x-\hat{i},y} \right] . \tag{2}
\end{aligned}$$

Here we follow the notation as in Ref. [11], where we have made the choice $r_t = r_s = 1$ for the Wilson parameters. Another parameter $\zeta = \kappa_s/\kappa_t$ is also commonly used in the literature. The forward and backward covariant derivatives on the lattice are given by:

$$\begin{aligned}
a_\mu \nabla_\mu \psi_x &= U_\mu(x) \psi_{x+\mu} - \psi_x , \\
a_\mu \nabla_\mu^* \psi_x &= \psi_x - U_\mu^\dagger(x - \mu) \psi_{x-\mu} . \tag{3}
\end{aligned}$$

Using these definitions, one can rewrite the fermion action (2) in continuum-like notations:

$$\begin{aligned}
S &= \sum_{xy} (a_t a_s^3) \bar{\psi}_x^{(c)} M_{xy}^{(c)} \psi_y^{(c)} , \\
M_{xy}^c &\equiv \frac{M_{xy}}{2\kappa_t a_t} = \left[m_0 + \frac{\zeta c_B}{2a_t} \sum_{i < j} \sigma_{ij} \mathcal{F}_{ij} + \frac{\zeta c_E}{2a_t} \sum_i \sigma_{0i} \mathcal{F}_{0i} \right] \delta_{xy} \\
&\quad + \gamma_0 \left(\frac{\nabla_0 + \nabla_0^*}{2} \right)_{xy} - \frac{a_t}{2} (\nabla_0 \nabla_0^*)_{xy} \\
&\quad + \sum_i \gamma_i \left(\frac{\nabla_i + \nabla_i^*}{2} \right)_{xy} - \frac{\xi \zeta a_s}{2} (\nabla_i \nabla_i^*)_{xy} , \tag{4}
\end{aligned}$$

where the the continuum fields and the bare quark mass m_0 are given by:

$$\begin{aligned}
\bar{\psi}_x &= a_s^{3/2} \frac{\bar{\psi}_x^{(c)}}{\sqrt{2\kappa_t}} , \quad \psi_x = a_s^{3/2} \frac{\psi_x^{(c)}}{\sqrt{2\kappa_t}} , \\
m_0 a_t &= \frac{1}{2\kappa_t} - 1 - 3\zeta . \tag{5}
\end{aligned}$$

For later convenience, we introduce the notation:

$$\nu = \xi \zeta , \quad \frac{1}{2\kappa} = \frac{\xi}{2\kappa_t} = m_0 a_s + \xi + 3\nu . \tag{6}$$

We call the parameter ν the bare speed of light parameter. The tuning of this parameter will be discussed in the remaining part of this paper using pseudo-scalar meson dispersion relations.

In quenched calculations, one usually needs to calculate the quark propagators at various valance quark masses. This amounts to different values of m_0 or κ for the same gauge field configuration. In this case, it is convenient to use the following fermion matrix:

$$\begin{aligned} \mathcal{M}_{xy} &= \delta_{xy}\sigma + \mathcal{A}_{xy} \\ \mathcal{A}_{xy} &= \delta_{xy} \left[1/(2\kappa_{max}) + \rho_t \sum_{i=1}^3 \sigma_{0i} \mathcal{F}_{0i} + \rho_s (\sigma_{12} \mathcal{F}_{12} + \sigma_{23} \mathcal{F}_{23} + \sigma_{31} \mathcal{F}_{31}) \right] \\ &\quad - \sum_{\mu} \eta_{\mu} \left[(1 - \gamma_{\mu}) U_{\mu}(x) \delta_{x+\mu,y} + (1 + \gamma_{\mu}) U_{\mu}^{\dagger}(x - \mu) \delta_{x-\mu,y} \right] , \end{aligned} \quad (7)$$

where the coefficients are given by:

$$\begin{aligned} \eta_i &= \frac{\nu}{2} , \quad \eta_0 = \frac{\xi}{2} , \quad \sigma = \frac{1}{2\kappa} - \frac{1}{2\kappa_{max}} , \\ \rho_t &= \nu \frac{(1 + \xi)}{4} , \quad \rho_s = \frac{\nu}{2} . \end{aligned} \quad (8)$$

Here we have used the tree-level, zero quark mass relation: [11]

$$c_B = 1 , \quad c_E = \frac{1 + \xi}{2} , \quad (9)$$

Note that, in principle the parameters c_B and c_E also have complicated dependence on the bare quark mass which we neglect in this study. In this notation, the bare quark mass dependence is singled out into parameter σ and the matrix \mathcal{A} remains *unchanged* when the bare quark mass is varied. Therefore, one could utilize the shifted structure of the matrix \mathcal{M} to solve for quark propagators at various values of m_0 (or equivalently κ) at the cost of solving only one value of $\kappa = \kappa_{max}$, using the so-called Multi-Mass Minimal Residual (M^3R for short) algorithm [29,30,31].

To implement the tadpole improvement, one replaces each spatial link $U_i(x)$ by $U_i(x)/u_s$ while keeping the temporal link unchanged.² This results in the same fermion matrix (7) except that the parameters are replaced by:

$$\begin{aligned} \eta_i &= \frac{\nu}{2u_s} , \quad \eta_0 = \frac{\xi}{2} , \quad \sigma = \frac{1}{2\kappa} - \frac{1}{2\kappa_{max}} , \\ \rho_t &= \nu \frac{(1 + \xi)}{4u_s^2} , \quad \rho_s = \frac{\nu}{2u_s^4} . \end{aligned} \quad (10)$$

² One can also introduce the tadpole improvement parameter u_t for the temporal link. For large anisotropy ξ , this turns out to be irrelevant since the temporal lattice spacing is small enough and for all practical purposes, one can set $u_t = 1$.

It is the quark action with these parameters that will be studied in this paper numerically.

3 Simulation Results

In this section, we present our numerical results for the study of the pseudo-scalar meson dispersion relations for various parameter sets (β, ν) . Our main focus lies upon the tuning of the bare speed of light parameter ν for a given gauge coupling β and a given type of meson. The parameter ν has to be tuned such that the energy-momentum dispersion relations of pseudo-scalar mesons under investigation reproduce the continuum form in the low-momentum limit. To achieve this goal, one has to go through several procedures which we will describe in the following.

3.1 Simulation parameters and meson correlation functions

The basic parameters of our simulation are summarized in Table 1. For the study of pseudo-scalar meson dispersion relations, it is advantageous to use lattices with asymmetric three-volume. This provides more non-degenerate (in the sense of its energy) low-momentum modes than the conventional symmetric lattices. All lattices in this study are of the size $6 \times 9 \times 12 \times 50$ except for the lattices at $\beta = 3.0$ where $8 \cdot 12 \cdot 16 \cdot 50$ lattices are studied.³ The aspect ratio of all lattices is $\xi = a_s/a_t \simeq \xi_0 = 5$. The value of β ranges between 2.2 and 3.0, roughly corresponding to spatial lattice spacing a_s between 0.12 and 0.27fm in physical units. For each particular value of β , gauge field configurations are generated using the conventional pseudo-heatbath algorithms with over-relaxation.

For gauge field configurations at a given value of β , 3 different values of the bare speed of light parameter ν as shown in Table 1 are studied. Quark propagators with zero and non-zero three-momenta are obtained using the M^3R algorithm with wall sources for each dirac and color index. With the help of the M^3R algorithm, by solving only one linear equation, one obtains the quark propagators with 12 (in the case of $\beta = 3.0$, only 8 values of κ were taken) different values of κ which correspond to different quark masses. The values of κ are chosen such that the quark mass values range roughly from around the

³ In our preliminary studies, $4 \times 6 \times 8 \times 40$ have also been simulated. We choose to present our results for larger lattices since they yield better accuracy for the pseudo-scalar meson dispersion relation measurements.

Table 1

Simulation parameters for lattices (all with $\xi = 5$) studied in this work. All lattices are of the size $6 \times 9 \times 12 \times 50$ except for $\beta = 3.0$ for which the lattice sizes are $8 \times 12 \times 16 \times 50$.

β	2.2			2.4			2.6		
	$r_0/a_s = 1.761$			$r_0/a_s = 2.180$			$r_0/a_s = 2.48$		
ν	0.86	0.90	0.94	0.85	0.90	0.94	0.87	0.90	0.93
κ	0.0630	0.0620	0.0605	0.0630	0.0620	0.0610	0.0630	0.0620	0.0615
	0.0625	0.0615	0.0600	0.0625	0.0615	0.0605	0.0625	0.0615	0.0610
	0.0620	0.0610	0.0595	0.0620	0.0610	0.0600	0.0620	0.0610	0.0605
	0.0615	0.0605	0.0590	0.0615	0.0605	0.0595	0.0615	0.0605	0.0600
	0.0605	0.0595	0.0580	0.0605	0.0595	0.0585	0.0605	0.0595	0.0590
	0.0590	0.0580	0.0565	0.0595	0.0585	0.0575	0.0590	0.0585	0.0580
	0.0575	0.0565	0.0550	0.0585	0.0575	0.0565	0.0575	0.0570	0.0565
	0.0560	0.0550	0.0535	0.0575	0.0565	0.0555	0.0565	0.0555	0.0555
	0.0545	0.0540	0.0525	0.0565	0.0555	0.0545	0.0555	0.0545	0.0545
	0.0540	0.0530	0.0520	0.0560	0.0550	0.0540	0.0550	0.0540	0.0540
	0.0535	0.0525	0.0515	0.0555	0.0545	0.0535	0.0545	0.0535	0.0535
	0.0530	0.0520	0.0510	0.0550	0.0540	0.0530	0.0540	0.0530	0.0530
	β	2.8			3.0				
$r_0/a_s = 3.13$			$r_0/a_s = 4.13$						
ν	0.87	0.90	0.93	0.87	0.90	0.93			
κ	0.0635	0.0625	0.0615	0.0635	0.0625	0.0615			
	0.0630	0.0620	0.0610	0.0630	0.0620	0.0610			
	0.0625	0.0615	0.0605	0.0625	0.0615	0.0605			
	0.0620	0.0610	0.0600	0.0620	0.0610	0.0600			
	0.0615	0.0600	0.0590	0.0600	0.0590	0.0580			
	0.0610	0.0590	0.0585	0.0580	0.0570	0.0560			
	0.0600	0.0580	0.0575	0.0575	0.0565	0.0555			
	0.0590	0.0570	0.0565	0.0570	0.0560	0.0550			
	0.0580	0.0565	0.0555						
	0.0570	0.0560	0.0550						
	0.0565	0.0555	0.0545						
	0.0560	0.0550	0.0540						

physical strange quark mass all the way up to the physical charm quark mass. The values of κ for each parameter set (β, ν) are also tabulated in Table 1.

In this paper, we focus on the single pseudo-scalar states with definite three-momentum. We define the pseudo-scalar and vector meson operators as follows:

$$P(\mathbf{x}, t) = \bar{q}_1(\mathbf{x}, t)\gamma_5 q_2(\mathbf{x}, t) , \quad (11)$$

where q_1, q_2 (\bar{q}_1, \bar{q}_2) are quark field operators of two (possibly identical) flavors. Operators which create meson states with definite three-momentum \mathbf{k} are then defined accordingly:

$$P(\mathbf{k}, t) = \frac{1}{\sqrt{V_3}} \sum_{\mathbf{x}} P(\mathbf{x}, t) e^{-i\mathbf{k}\cdot\mathbf{x}} , \quad (12)$$

where V_3 designates the three-volume of the lattice. Using these operators, one constructs the corresponding meson correlation function:

$$C^{(PS)}(\mathbf{k}, t) = \langle P(\mathbf{k}, t)^\dagger P(\mathbf{k}, 0) \rangle , \quad (13)$$

Using Wick's theorem, the above defined correlation function can be expressed in terms of the quark propagators:

$$C^{(PS)}(\mathbf{k}, t) = \frac{1}{V_3} \sum_{\mathbf{y}} Y_{\beta a y t}^{(1)\rho b} \left[X_{\alpha a y t}^{(2)\sigma b} \right]^* \cdot e^{i\mathbf{k}\cdot\mathbf{y}} , \quad (14)$$

where the Greek subscripts/superscripts in the solution vectors X and Y are Dirac indices while Roman subscripts/superscripts are color indices. The solution vectors X and Y are given by the inverse fermion matrix elements:

$$\begin{aligned} Y_{\beta a y t}^{\rho b} &= \sum_{\mathbf{x}} \mathcal{M}_{\beta a y t; \rho b \mathbf{x} 0}^{-1} e^{-i\mathbf{k}\cdot\mathbf{x}} , \\ X_{\beta a y t}^{\rho b} &= \sum_{\mathbf{x}} \mathcal{M}_{\beta a y t; \rho b \mathbf{x} 0}^{-1} . \end{aligned} \quad (15)$$

The superscript (1) or (2) on these solution vectors indicates that the quark mass should be that of quark flavor 1 or 2 (possibly identical). These solution vectors are obtained by solving the linear equation of the fermion matrix \mathcal{M} with a suitable wall source.

Then energy of a pseudo-scalar meson with definite three-momentum \mathbf{k} (including zero-momentum) is obtained from their respective correlation functions $C^{(PS)}(\mathbf{k}, t)$ by finding the plateaus in their effective mass plots. In Fig. 1, we show the effective mass plots of a pseudo-scalar consisting of a quark and an anti-quark with the same quark mass for the parameter set $\beta = 2.4$, $\nu = 0.9$. There are 8 small windows in this plot, each containing the effective mass plot of the pseudo-scalar meson state with various three-momentum: $\mathbf{n} = (0, 0, 0)$, $(1, 0, 0)$, $(0, 1, 0)$, $(0, 0, 1)$, $(1, 1, 0)$, $(1, 0, 1)$, $(0, 1, 1)$ and $(1, 1, 1)$ (see Eq. (18) and Eq. (19) for notations) which are also labelled in each window. There are 12 lines in each of these windows which correspond to 12 different values of the quark mass. It is seen that all effective mass plots develop nice plateaus at large temporal separation and accurate values of the pseudo-scalar energy $E_{PS}(\mathbf{k})$ can thus be extracted. The errors for the data points in this plot are analyzed using the standard jack-knife method. The intervals from which we extract the energy values are self-adjusted according to the minimum of χ^2 per degree of freedom. These intervals are indicated in the figure by red horizontal line segments. The quality of the effective mass plots for other parameter sets are quite similar.

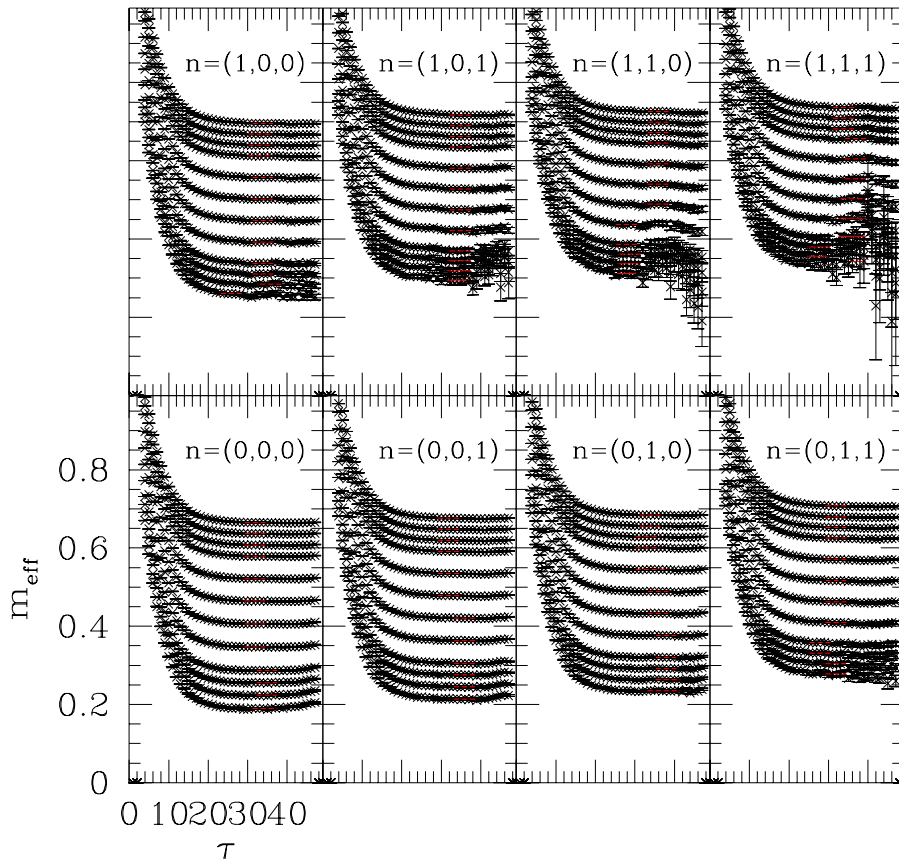


Fig. 1. The effective mass plots for the pseudo-scalar meson made up of a quark and an anti-quark with the same mass for definite three-momenta at $\beta = 2.4, 0.90$. The windows corresponds to three momentum label (as Eq. (19)) of $\mathbf{n} = (0, 0, 0), (1, 0, 0), (0, 1, 0), (0, 0, 1), (1, 1, 0), (1, 0, 1), (0, 1, 1)$ and $(1, 1, 1)$, respectively. Different lines in each window correspond to different quark mass values.

3.2 Fixing the strange and charm quark mass

We now describe how to fix the hopping parameters which correspond to the physical strange and charm quark mass. The masses for the pseudo-scalar mesons are obtained for various quark mass values at a given set of (β, ν) . These results enable us to make a chiral extrapolation to determine the critical hopping parameter κ_{cr} at which the pseudo-scalar (pion) becomes massless. In this paper, we have adopted a quadratic fitting function of the form:

$$a_t^2 m_\pi^2 = B_\pi \left(\frac{1}{2\kappa} - \frac{1}{2\kappa_{cr}} \right) + C_\pi \left(\frac{1}{2\kappa} - \frac{1}{2\kappa_{cr}} \right)^2, \quad (16)$$

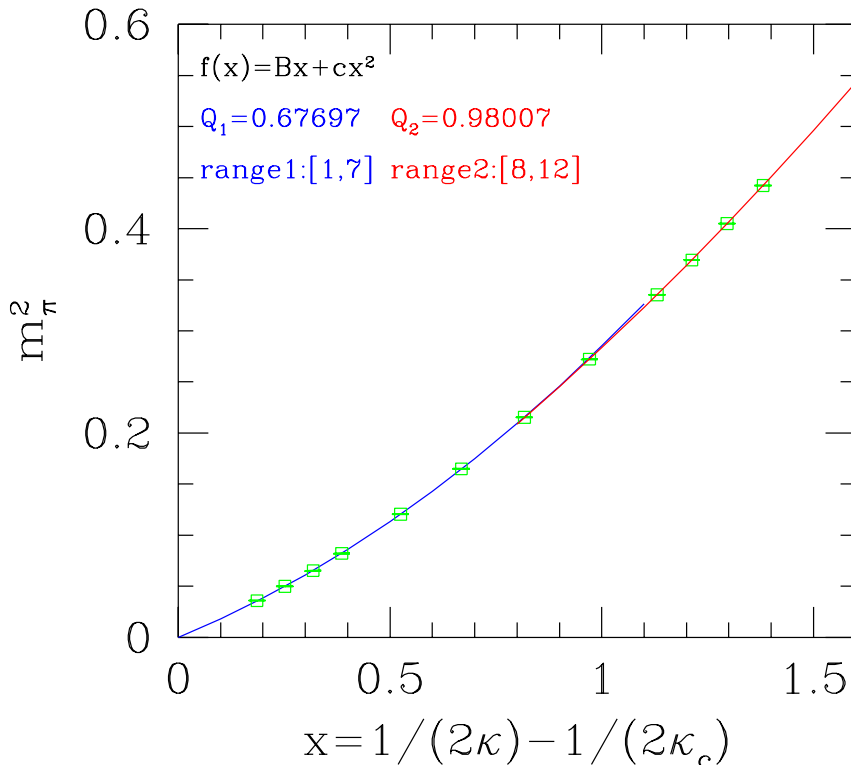


Fig. 2. Chiral extrapolation of the pseudo-scalar meson consisting of equal mass quark and anti-quark at $\beta = 2.4$, 0.90 . The data points are values of m_{PS}^2 obtained from corresponding effective mass plateaus. These data can be fitted with two quadratic functions in the low quark mass region (blue curve) and the high quark mass region (red curve) separately. The fitting ranges are also listed. From the fit in the low quark mass region, one infers the value of $1/(2\kappa_{cr})$.

This yields the pseudo-scalar mass in lattice units in the small quark mass region. In Fig. 2, a typical chiral extrapolation for the pion mass squared is shown versus the quark mass parameter $x = 1/(2\kappa) - 1/(2\kappa_{cr})$ for the parameter set $\beta = 2.4$, $\nu = 0.90$. The data points in the plot are obtained from the corresponding effective mass plateaus in Fig 1 and the blue curve represents the chiral extrapolation using the quadratic fit (16). In most of our study we have taken 12 values of bare quark mass. We find that the quark mass dependence of physical quantities (like the pion mass squared) can be fitted using two quadratic functions in the low (blue curve) and high (red curve) quark mass region separately. For the chiral extrapolation we are concerned

with the quadratic fit in the low quark mass region. The fitting range for the chiral extrapolation is self-adjusted from the small quark end of the data to yield minimum χ^2 for each degree of freedom. The optimal choice of the fitting range is also labelled in the figure together with the quality of the fit Q . Note that the fitted parameters: κ_{cr} , B_π and C_π which enter the above chiral extrapolation still depend on the parameter set (β, ν) . The results of $1/(2\kappa_{cr})$ for each parameter set are tabulated in Table 2. In what follows, we will use the notation:

$$x \equiv \frac{1}{2\kappa} - \frac{1}{2\kappa_{cr}} \quad (17)$$

and call it the quark mass parameter. Physical properties of a meson will depend on one or two quark mass parameter(s) depending on whether the meson is made up of a quark and an anti-quark with equal mass or not.

The physical strange quark mass parameter $x_s^{(phy)}$ can be determined from the so-called K -input. In this procedure, one investigates the pseudo-scalar meson made up of two different flavors (therefore different masses) of quarks. The mass squared of such a pseudo-scalar meson (kaon) $m_{PS}^2(x_1, x_2)$ hence depends on two quark mass parameters: x_1 and x_2 . To fix the physical strange quark mass parameter $x_s^{(phy)}$, one first extrapolates one of the quark mass parameters (say x_2) to zero quark mass (chiral limit) and then inspects the dependence of the pseudo-scalar meson mass squared $m_{PS}^2(x_1, 0)$ on the other quark mass parameter x_1 . The physical strange quark mass parameter $x_s^{(phy)}$ is determined by demanding that the mass of the pseudo-scalar meson reproduces the corresponding experimental value. Here one has to set the physical scale using some method. In this work, we choose the hadronic scale $r_0 = 0.5\text{fm}$ (the so-called Sommer scale) obtained from heavy quark anti-quark potential.⁴ For different values of gauge coupling β , the values of r_0/a_s are known from the literature [2,3] which are also listed in Table 1 for reference. Therefore, by fitting the pseudo-scalar meson mass squared $m_{PS}^2(x_1, 0)$ as a quadratic function of the quark mass parameter x_1 , we extract the physical value for the parameter $x_s^{(phy)}$. As an illustration, this procedure is shown in Fig. 3 for one of our data sets: $\beta = 2.4$, $\nu = 0.90$. In the upper panel of this figure, we plotted the pseudo-scalar mass squared $m_{PS}^2(x_1, x_2)$ versus the quark mass parameter x_2 with the other quark mass parameter x_1 being fixed. These data points are fitted with a quadratic function in x_2 and the fitted results are shown as curves in the upper panel of the figure. From these fits, we have the pseudo-scalar mass squared with one quark mass parameter extrapolated to zero: $m_{PS}^2(x_1, 0)$. In the lower panel of the figure, we plot the result of $m_{PS}^2(x_1, 0)$ versus the other quark mass parameter x_1 . The data points are again fitted by

⁴ We have assumed that $r_0 = 0.5\text{fm}$ exactly. Therefore, errors in this scale are not taken into account in the following error analysis.

Table 2

Extracted physical quark mass parameters and the Z factors for D , D_s and η_c pseudo-scalar mesons for all (β, ν) sets. The numbers in the square brackets after each ν value indicate the number of configurations measured. The final values for the optimized parameters ν_{opt} are also given in the final row of the table for every β .

β	2.2			2.4		
ν	0.86[304]	0.90[303]	0.94[304]	0.85[303]	0.90[302]	0.94[303]
$1/(2\kappa_{cr})$	7.337(4)	7.86(2)	8.048(5)	7.682(6)	7.878(5)	8.028(5)
$x_s^{(phy)}$	0.2041(33)	0.227(14)	0.1947(40)	0.140(20)	0.131(13)	0.1384(88)
$x_c^{(phy)}$	1.879(2)	1.583(5)	1.834(1)	1.4287(8)	1.401(1)	1.3866(7)
$Z_{PS}[x_c^{(phy)}, x_c^{(phy)}]$	1.32(5)	1.40(3)	1.47(1)	1.26(2)	1.36(2)	1.43(2)
$Z_{PS}[x_c^{(phy)}, 0]$	1.20(9)	1.40(18)	1.41(9)	1.13(3)	1.15(2)	1.27(3)
$Z_{PS}[x_c^{(phy)}, x_s^{(phy)}]$	1.21(5)	1.31(3)	1.35(2)	1.12(2)	1.17(1)	1.27(3)
$\nu_{opt}^D, \nu_{opt}^{D_s}, \nu_{opt}^{\eta_c}$	0.78(8), 0.72(8), 0.68(7)			0.78(4), 0.78(2), 0.71(3)		
β	2.6			2.8		
ν	0.87[303]	0.90[304]	0.93[303]	0.87[304]	0.90[303]	0.93[304]
$1/(2\kappa_{cr})$	7.765(4)	7.879(5)	7.998(4)	7.762(2)	7.865(4)	7.990(3)
$x_s^{(phy)}$	0.1227(75)	0.117(15)	0.1111(79)	0.095(2)	0.119(3)	0.097(3)
$x_c^{(phy)}$	1.191(1)	1.179(3)	1.1612(9)	0.9056(7)	0.905(1)	0.8850(8)
$Z_{PS}[x_c^{(phy)}, x_c^{(phy)}]$	1.313(4)	1.368(5)	1.421(4)	1.25(1)	1.295(8)	1.36(1)
$Z_{PS}[x_c^{(phy)}, 0]$	1.196(8)	1.236(9)	1.255(8)	1.17(1)	1.19(4)	1.28(3)
$Z_{PS}[x_c^{(phy)}, x_s^{(phy)}]$	1.204(6)	1.248(7)	1.273(5)	1.162(7)	1.19(2)	1.27(1)
$\nu_{opt}^D, \nu_{opt}^{D_s}, \nu_{opt}^{\eta_c}$	0.67(5), 0.69(2), 0.69(1)			0.78(3), 0.78(2), 0.74(2)		
β	3.0					
ν	0.87[295]	0.90[300]	0.93[300]			
$1/(2\kappa_{cr})$	7.765(1)	7.856(3)	7.972(3)			
$x_s^{(phy)}$	0.0378(3)	0.0636(83)	0.563(81)			
$x_c^{(phy)}$	0.6486(4)	0.6625(4)	0.6499(4)			
$Z_{PS}[x_c^{(phy)}, x_c^{(phy)}]$	1.17(1)	1.22(1)	1.28(1)			
$Z_{PS}[x_c^{(phy)}, 0]$	1.06(1)	1.11(2)	1.16(1)			
$Z_{PS}[x_c^{(phy)}, x_s^{(phy)}]$	1.07(1)	1.12(2)	1.17(2)			
$\nu_{opt}^D, \nu_{opt}^{D_s}, \nu_{opt}^{\eta_c}$	0.82(3), 0.82(2), 0.78(2)					

a quadratic function in x_1 which is shown as the blue curve in the lower panel. The fitting interval and the quality of the fit are also shown. The horizontal line in the lower panel represents the experimental value of kaon mass squared with the scale being set by r_0 . This horizontal line intersects with the fitted blue curve. The point of intersection then gives the estimate for the physical strange quark mass parameter $x_s^{(phy)}$ together with its error. This is indicated in the figure by a solid circle. The values of $x_s^{(phy)}$ for each parameter set (β, ν) and the corresponding errors are listed in Table 2. Just like the pion chiral extrapolation, the optimal interval of the fits in this process are obtained by the requirement of minimum χ^2 per degree of freedom.

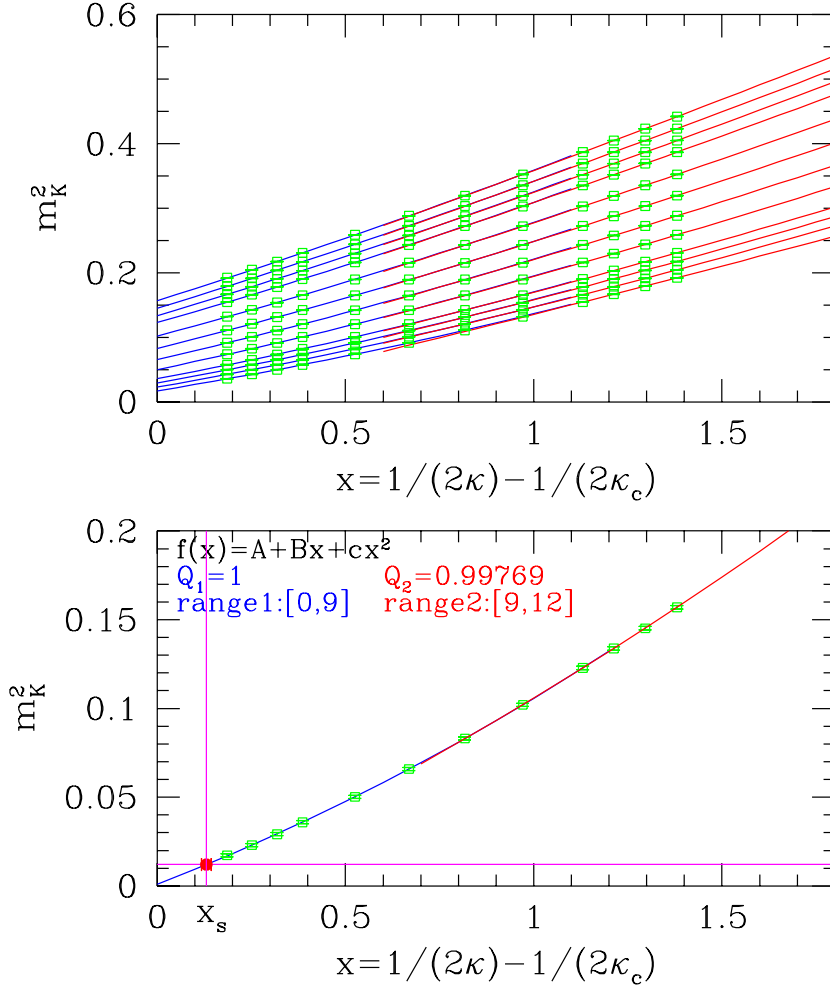


Fig. 3. Chiral extrapolation and the determination of the physical quark mass parameter with K -input at $\beta = 2.4, 0.90$. In the upper panel of the figure, pseudo-scalar mass squared $m_{PS}^2(x_1, x_2)$ is plotted versus the quark mass parameter x_2 for each fixed x_1 . The chiral extrapolated results $m_{PS}^2(x_1, 0)$ are shown in the lower panel of the figure versus the other quark mass parameter x_1 . Chiral extrapolation with respect to x_1 is shown as the blue curve from which one can read off the physical strange quark mass parameter $x_s^{(phy)}$ (shown as the solid circle with error).

The physical charm quark mass, or equivalently the corresponding hopping parameter κ_c , is determined by demanding that the spin-averaged charmonium mass $(m_{\eta_c} + 3m_{J/\psi})/4$ reproduces the corresponding experimental value 3067.6 MeV. In Fig. 4, we plot the spin-averaged meson mass squared versus the quark mass parameter x . The data points are fitted using a quadratic function in the quark mass parameter x which is shown as the red curve. For the case of the charm quark mass, this fit starts from the side with heavier quark masses, as opposed to the case of the kaon where we start from the side

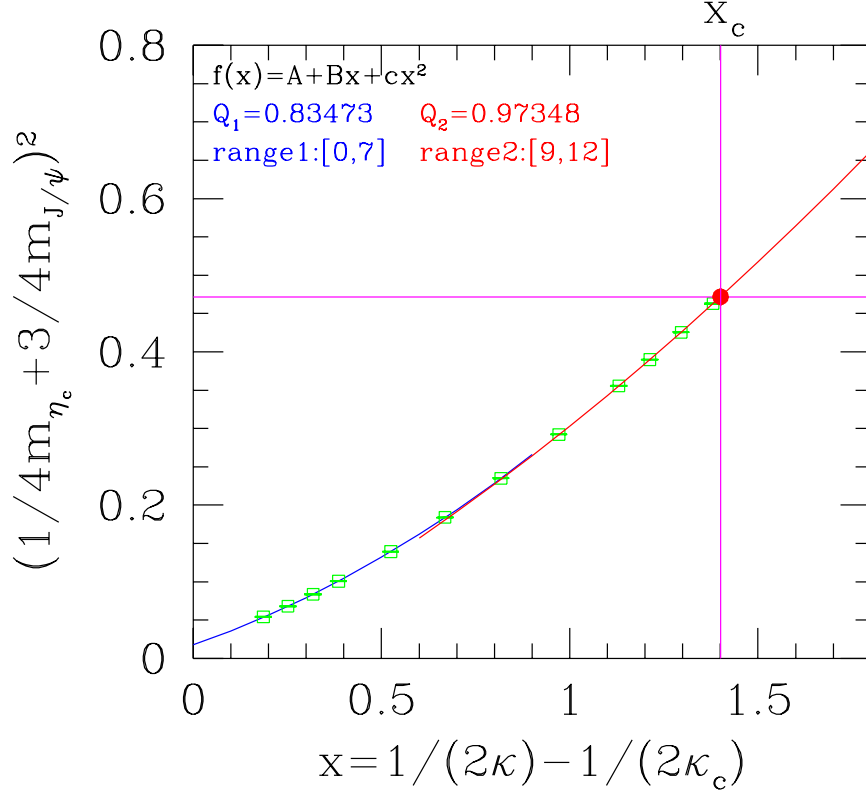


Fig. 4. Determination of the physical charm quark mass at $\beta = 2.4, 0.90$. The spin-averaged charmonium mass squared is plotted versus the quark mass parameter x . The red curve represents a quadratic fit in the heavy quark mass range. The horizontal line is the corresponding experimental value and the intersection point gives the physical charm quark mass parameter $x_c^{(phy)}$ which is shown as a solid circle with error.

with lighter quark masses. Fitting intervals are self-adjusted as before and the optimal range is indicated in the plot together with the quality of the fit Q . The horizontal line represents the corresponding experimental value and the intersection with the fitted curve yields the corresponding physical charm quark mass parameter $x_c^{(phy)}$ which is shown as the solid circle in the figure. The results of $x_s^{(phy)}$ and $x_c^{(phy)}$ for all parameter set (β, ν) are listed in Table 2 for reference.

3.3 Extraction of Z parameter

In this work, we utilize lattices with asymmetric volumes. This asymmetry helps to break the cubic symmetry in the momentum space and lifts the degeneracy of the meson energies. For example, by using a lattice of size $6 \times 9 \times 12 \times 50$, we have 8 non-degenerate low-momentum modes, compared with only 4 with symmetric volumes. This technique also proves to be useful for the measurement of other momentum-dependent quantities like the hadron-hadron scattering phase shifts [32,33]. The three-momenta \mathbf{k} in an asymmetric box of size $L_1 \times L_2 \times L_3$ ⁵ are quantized according to:

$$\mathbf{k} = \left(\frac{2\pi}{L_1}n_1, \frac{2\pi}{L_2}n_2, \frac{2\pi}{L_3}n_3 \right), \quad (18)$$

with $\mathbf{n} = (n_1, n_2, n_3) \in \mathbb{Z}^3$ being three-dimensional integers. In this work, the energy values of a meson with the following 8 three-momentum are measured:

$$\begin{aligned} \mathbf{n} = & (0, 0, 0), (0, 0, 1), (0, 1, 0), (1, 0, 0), \\ & (0, 1, 1), (1, 0, 1), (1, 1, 0), (1, 1, 1). \end{aligned} \quad (19)$$

For a given three-momentum \mathbf{k} , the pseudo-scalar meson energy levels $E_{PS}(\mathbf{k})$ are fitted according to the expected continuum dispersion relation:

$$E_{PS}^2(\mathbf{k}) = m_{PS}^2 + Z_{PS}\mathbf{k}^2, \quad (20)$$

in the low-momentum region. The fitting is performed for pseudo-scalar mesons with possibly two different flavors of quarks. As a result of these fits, we obtain all the Z parameters of the pseudo-scalar mesons as a function of possibly two quark mass parameters: $Z_{PS}(x_1, x_2)$.⁶ In Fig. 5, the fit of dispersion relations of the pseudo-scalar meson with equal mass quark and anti-quark are shown for $\beta = 2.4$, $\nu = 0.9$. The straight lines represent the linear fits for 12 κ values using the low-momentum data points (including the zero-momentum point) according to Eq. (20). The fitting range is self-adjusted to yield the minimum χ^2 for each degree of freedom. The slope of these lines then gives the parameters $Z_{PS}(x, x)$ for all quark mass parameter x . Fitting qualities for other (β, ν) are quite similar. We have also tried another (conventional) way of extracting $Z_{PS}(x, x)$, namely by using only the zero-momentum point and the

⁵ For definiteness, we pick $L_1 \leq L_2 \leq L_3$.

⁶ For the pseudo-scalar meson made up of quarks with the same mass, the corresponding Z parameter then only depends on one quark mass parameter, namely $Z_{PS}(x, x)$.

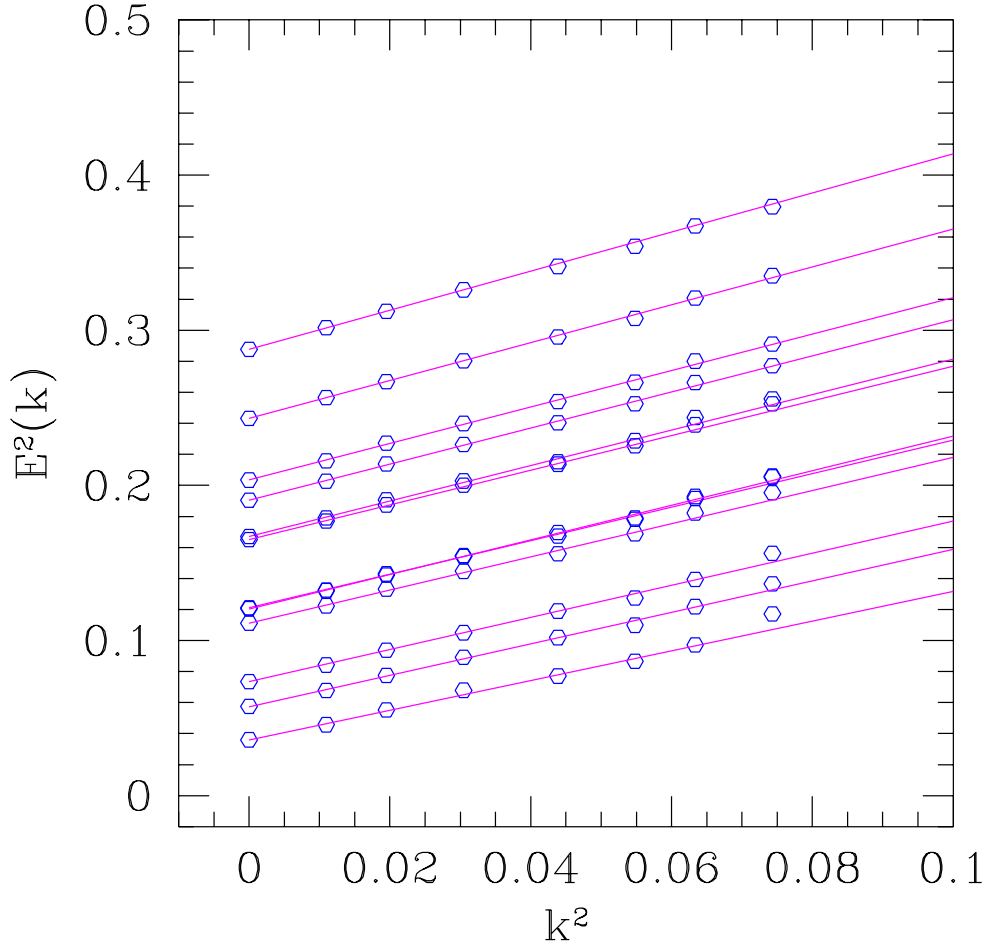


Fig. 5. Dispersion relations of the pseudo-scalar meson consisting of equal mass quark and anti-quark at $\beta = 2.4, 0.90$. The data points show the pseudo-scalar meson energy squared $E_{PS}^2(\mathbf{k})$ at a given three-momentum \mathbf{k} versus \mathbf{k}^2 . The straight lines are the linear fits to the data with the fitting range starting from the low-momentum end and self-adjusted according to the minimum χ^2 per degree of freedom. The slope of the lines then yield the desired Z parameters.

lowest non-vanishing momentum point $(0, 0, 1)$. This is what has been done in the literature by many authors [12,24,25,26]. We find that the Z parameters are always better determined by using linear fits with more momentum points as compared with only two lowest momentum points. Therefore, we see the advantage of using asymmetric volumes for all our parameter sets.

3.4 Tuning of the bare speed of light parameter

The optimal choice for the bare speed of light parameter ν is determined from the corresponding pseudo-scalar meson dispersion relations, or more explicitly, from the Z parameters $Z_{PS}(x_1, x_2)$ extracted from dispersion relations which is discussed the previous subsection. For a particular type of pseudo-scalar meson under investigation, one requires that the dispersion relation of the meson reproduces its continuum counter-part in the low-momentum limit. That is to say, the optimal choice of ν has to be such that:

$$Z_{PS}(\nu_{opt}) = 1 . \quad (21)$$

For definiteness, we focus on the following three situations: a) pseudo-scalar meson with the same type of quark whose mass is the charm quark mass; b) pseudo-scalar meson with two different types of quark with one being the charm, the other mass close to zero; c) pseudo-scalar meson with two different types of quark with one mass being that of charm, the other being that of strange. These situations are physically more interesting since they correspond to η_c meson, D meson and D_s meson, respectively. We now proceed to discuss these three situations.

For the case of pseudo-scalar meson consisting of the same flavor, the extracted parameter $Z_{PS}(x, x)$ is plotted against the quark mass parameter x . In Fig. 6, we show this plot for $\beta = 2.4$, $\nu = 0.90$ lattices. These results can be fitted in the low quark mass region (blue curve) and in the high quark mass region (red curve) separately, using quadratic functions in the quark mass parameter x . The fits are represented by the two curves in the figure. For the quadratic fits in the high quark mass region (red curve), if we plug in the physical charm quark mass parameter $x_c^{(phy)}$ determined from the meson mass, we get the Z parameter at the physical charm mass: $Z_{PS}(x_c^{(phy)}, x_c^{(phy)})$ which is the Z parameter for the physical η_c meson. This is shown in the figure as a solid circle together with its error. Since the parameter $x_c^{(phy)}$ depends on ν , for a given value of β , we therefore obtain three values of $Z_{PS}[x_c^{(phy)}(\nu), x_c^{(phy)}(\nu)]$ corresponding to 3 different values of ν being investigated. The values of $Z_{PS}(x_c^{(phy)}, x_c^{(phy)})$ for all (β, ν) are listed in Table 2.

For the pseudo-scalar meson D , we first extrapolate one of the quark mass parameter, say x_2 , in $Z_{PS}(x_1, x_2)$ to zero (chiral limit), for every fixed value of x_1 . As a result, we have $Z_{PS}(x_1, 0)$ available. In the second step, we extrapolate/interpolate $Z_{PS}(x_1, 0)$ as a quadratic function in x_1 in the high quark mass region. Finally, we plug in the physical value of $x_1 = x_c^{(phy)}$ which then yields the final result $Z_{PS}[x_c^{(phy)}(\nu), 0]$ for the D meson for all parameter sets (β, ν) . In Fig. 7, we illustrate this procedure for $\beta = 2.4$, $\nu = 0.9$. In this figure, the extrapolated results $Z_{PS}(x_1, 0)$ are shown as a function of x_1 and

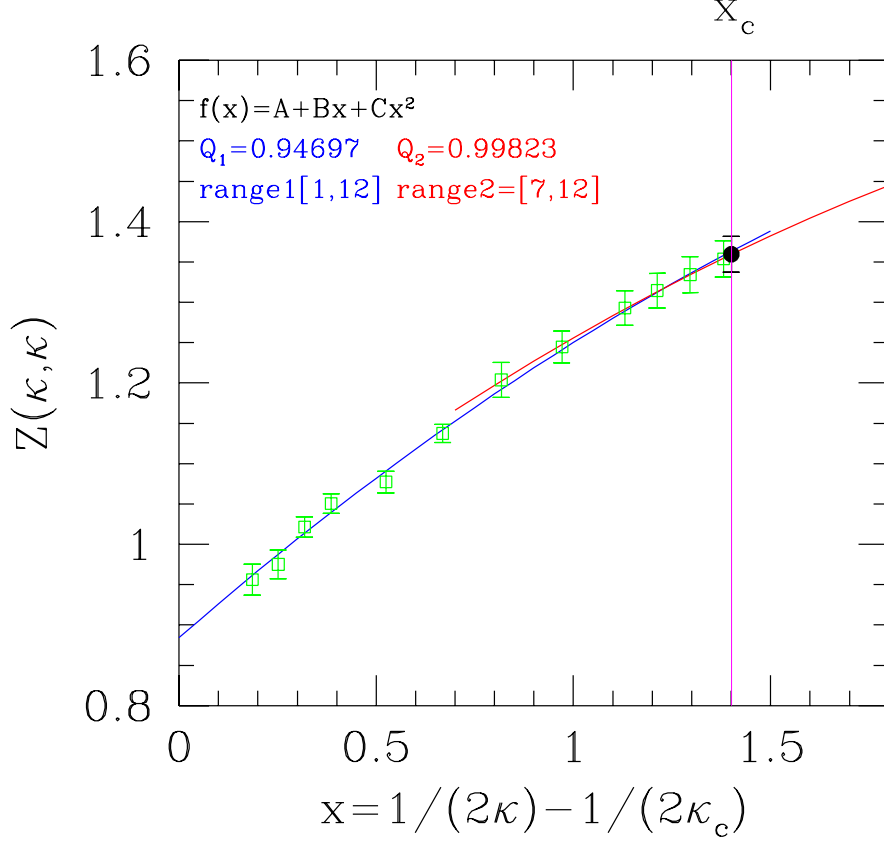


Fig. 6. The determination of $Z_{PS}[x_c^{(phy)}(\nu), x_c^{(phy)}(\nu)]$ at $\beta = 2.4, 0.90$. The red curve is a quadratic fit in the high quark mass region and the value of $Z_{PS}[x_c^{(phy)}(\nu), x_c^{(phy)}(\nu)]$ is shown as the solid circle with error.

it is extrapolated versus x_1 in the high quark mass region (red curve) using a quadratic function. The position of the physical charm quark mass parameter is also indicated and the final result of $Z_{PS}[x_c^{(phy)}(\nu), 0]$ is shown as a solid circle in the figure. Results of $Z_{PS}[x_c^{(phy)}(\nu), 0]$ for all parameter sets are also listed in Table 2.

Following a similar procedure, we obtain the Z parameter for the D_s meson: $Z_{PS}[x_c^{(phy)}(\nu), x_s^{(phy)}(\nu)]$ for each parameter set (β, ν) . In Fig. 8, we show an illustration at $\beta = 2.4, \nu = 0.9$. The results of $Z_{PS}[x_c^{(phy)}(\nu), x_s^{(phy)}(\nu)]$ for all parameter sets are also listed in Table 2.

After obtaining the results for Z at physical quark mass values for three different values of ν , one can further make a extrapolation/interpolation in ν . This is

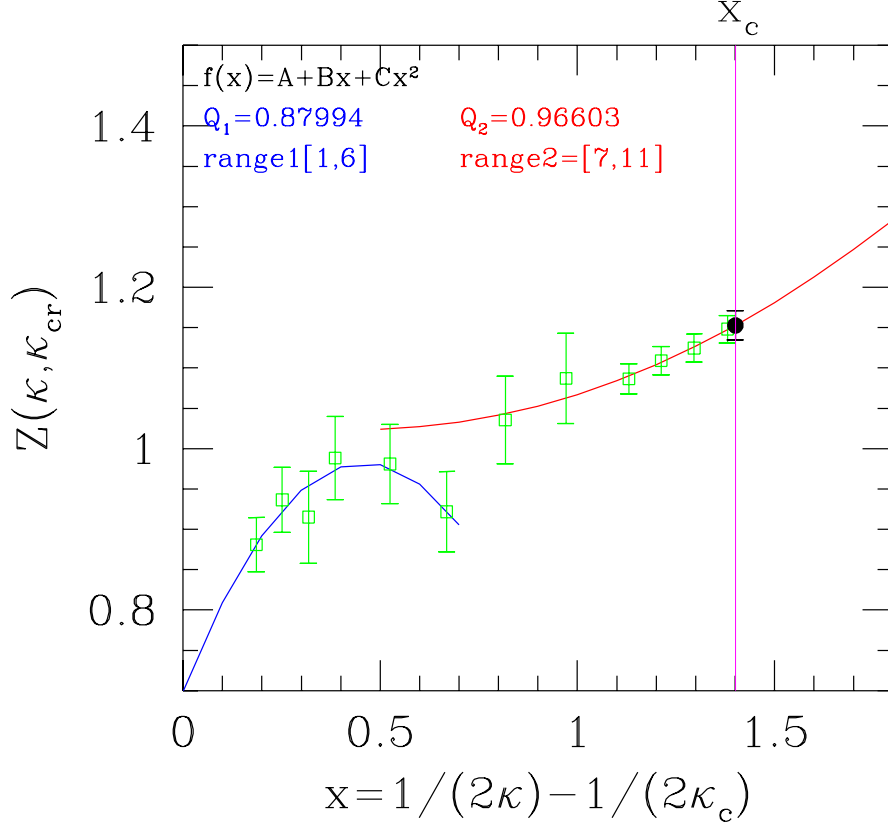


Fig. 7. The determination of $Z_{PS}[x_c^{(phy)}(\nu), 0]$ with $\beta = 2.4, 0.90$. The extrapolated results $Z_{PS}(x_1, 0)$ are shown as data points in the figure versus x_1 . They are fitted in the high quark mass region with a quadratic function in x_1 (red curve). The vertical line shows the position of the physical charm quark mass parameter. Thus, $Z_{PS}[x_c^{(phy)}, 0]$ is determined which is indicated as a solid circle with error.

done separately for the three cases of $Z_{PS}[x_c^{(phy)}(\nu), 0]$, $Z_{PS}[x_c^{(phy)}(\nu), x_s^{(phy)}(\nu)]$ and $Z_{PS}[x_c^{(phy)}(\nu), x_c^{(phy)}(\nu)]$ for every value of β . Requiring the corresponding $Z_{PS}(\nu) = 1$ then yields an estimate for the optimal value for the parameter ν for each case. In Fig. 9, Fig. 10 and Fig. 11 the extrapolations in ν for all 5 values of β are shown for D , D_s and η_c mesons, respectively. The straight lines in these figures are the linear extrapolation in ν and the final results for ν_{opt} are indicated as solid circles with errors. These results are also tabulated in Table 2 for every β .

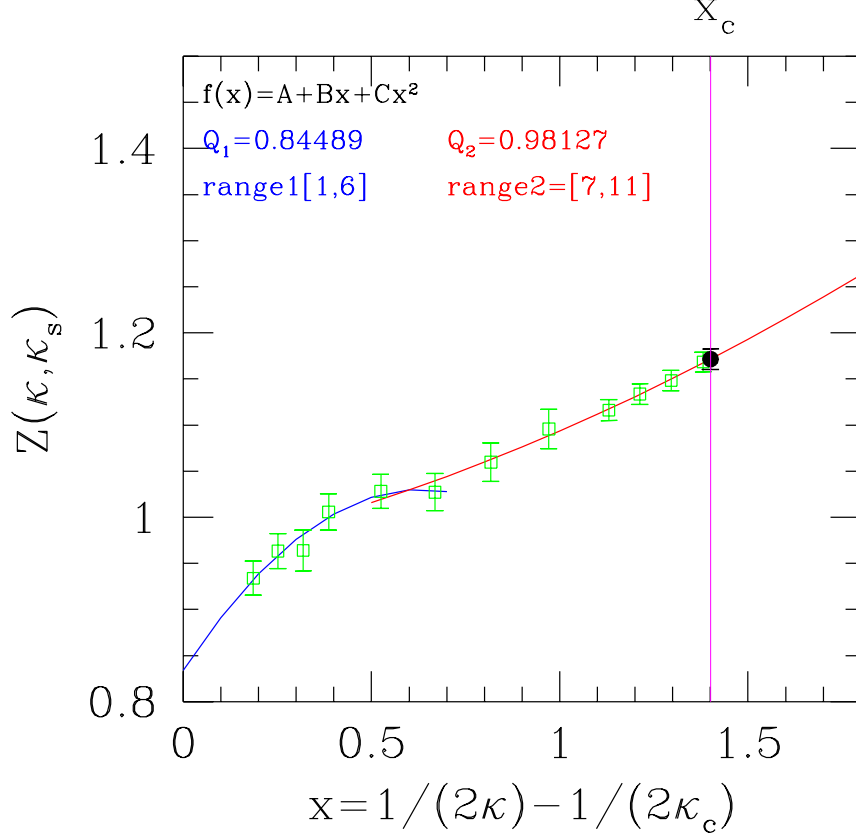


Fig. 8. The determination of $Z_{PS}[x_c^{(phy)}(\nu), x_s^{(phy)}(\nu)]$ with $\beta = 2.4, 0.90$. The extrapolated results $Z_{PS}(x_1, x_s^{(phy)})$ are shown as data points in the figure versus the quark mass parameter x_1 . They are fitted in the high quark mass region with a quadratic function in x_1 (red curve). The vertical line shows the position of the physical charm quark mass parameter. Thus, $Z_{PS}[x_c^{(phy)}, x_s^{(phy)}]$ is determined which is indicated as a solid circle with error.

4 Conclusions

In this paper, we present a systematic numerical analysis on the tuning of the bare speed of light parameter in the anisotropic Wilson quark action. The tuning is done in a quark mass dependent way with quark mass values ranging from the strange to the charm. The optimal values of ν are obtained for various values of β using the η_c , D and D_s meson dispersion relations. With the help of the anisotropic lattices with asymmetric volumes, the dispersion relations can be measured with good accuracy. Using the improved anisotropic

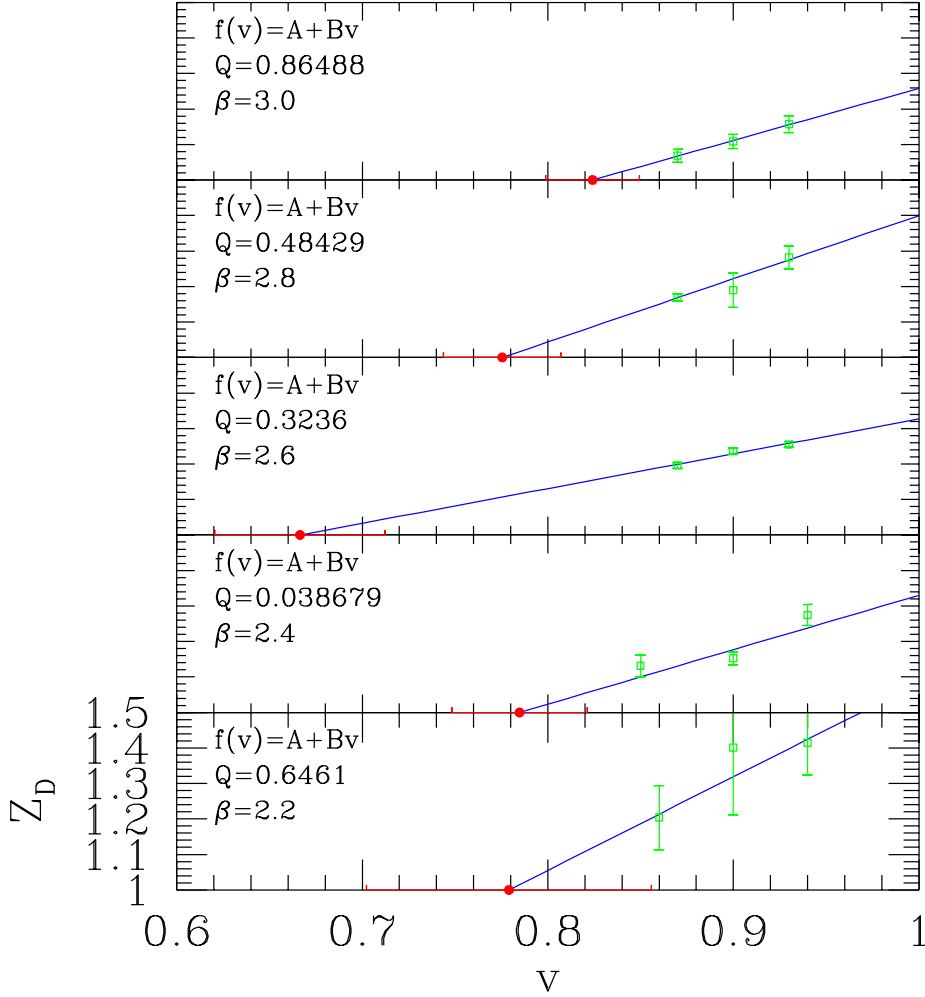


Fig. 9. The determination of optimal value ν_{opt} for D meson at various values of β . The straight lines are the linear extrapolation in ν and the final results for ν_{opt} are indicated as solid circles with errors.

Wilson action with these optimized parameters, a quenched calculation can then be performed to study properties of hadrons made up of either light or heavy quarks. Therefore, with the same improved quark action one can study hadron spectrum and other physical properties in a wide range of quark masses. We hope to come to this issue in the near future.

Acknowledgments

We would like to thank Prof. H. Q. Zheng and Prof. S. L. Zhu of Peking University for helpful discussions. Our thanks also goes to Dr. J.P. Ma at Institute of Theoretical Physics, Academia Sinica and Dr. Y. Chen at Institute

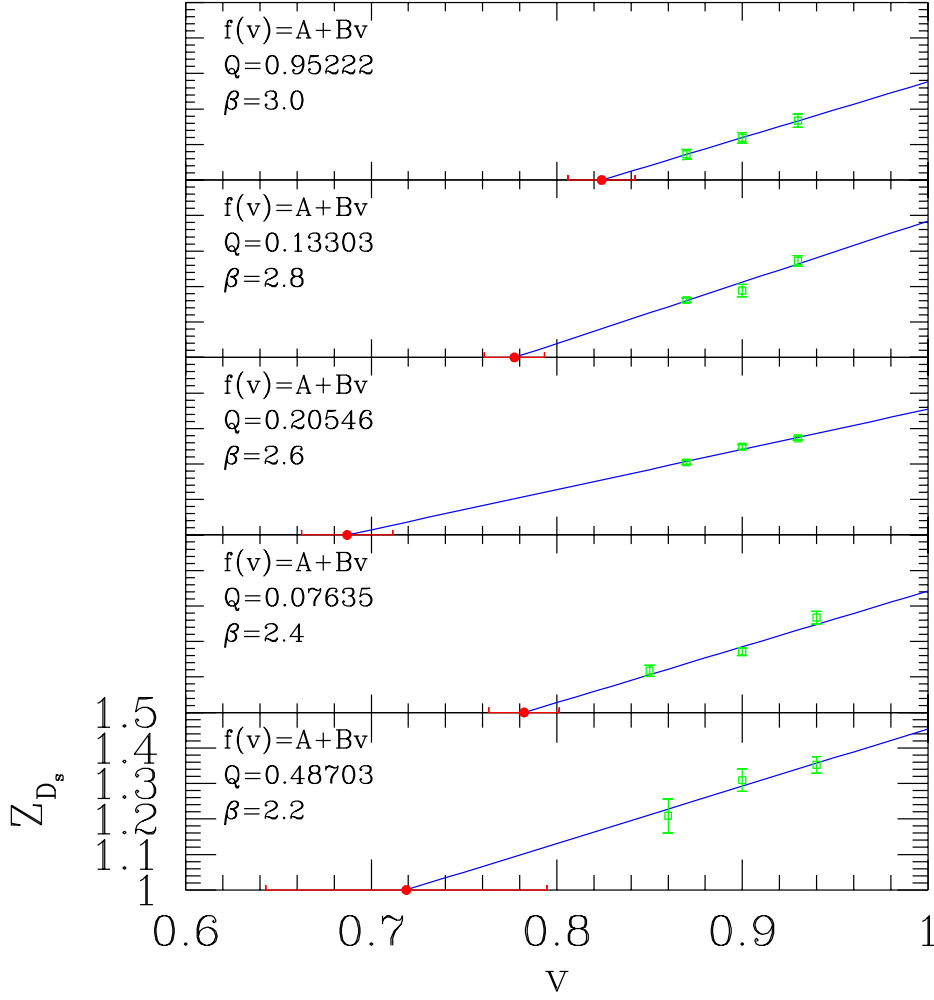


Fig. 10. The determination of optimal value ν_{opt} for D_s meson at various values of β . The straight lines are the linear extrapolation in ν and the final results for ν_{opt} are indicated as solid circles with errors.

of High Energy Physics, Academia Sinica for their stimulating discussions.

References

- [1] C. Morningstar and M. Peardon. *Phys. Rev. D*, 56:4043, 1997.
- [2] C. Morningstar and M. Peardon. *Phys. Rev. D*, 60:034509, 1999.
- [3] C. Liu. *Chinese Physics Letter*, 18:187, 2001.
- [4] C. Liu. *Communications in Theoretical Physics*, 35:288, 2001.
- [5] C. Liu. In *Proceedings of International Workshop on Nonperturbative Methods and Lattice QCD*, page 57. World Scientific, Singapore, 2001.

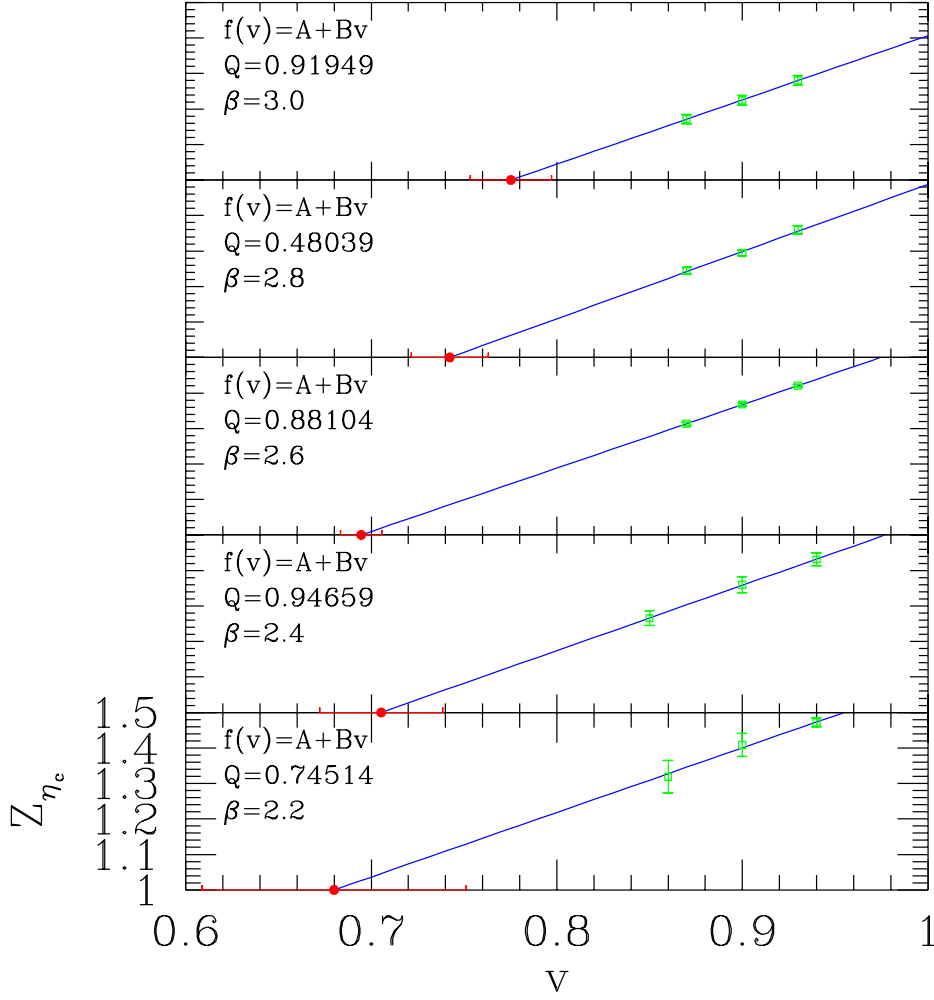


Fig. 11. The determination of optimal value ν_{opt} for η_c meson at various values of β . The straight lines are the linear extrapolation in ν and the final results for ν_{opt} are indicated as solid circles with errors.

- [6] C. Liu and J. P. Ma. In *Proceedings of International Workshop on Nonperturbative Methods and Lattice QCD*, page 65. World Scientific, Singapore, 2001.
- [7] C. Liu. *Nucl. Phys. (Proc. Suppl.) B*, 94:255, 2001.
- [8] A.X. El-Khadra, A.S. Kronfeld, and P.B. Mackenzie. *Phys. Rev. D*, 55:3933, 1997.
- [9] M. Alford, T. R. Klassen, and P. Lepage. *Phys. Rev. D*, 58:034503, 1998.
- [10] T. R. Klassen. *Nucl. Phys. (Proc. Suppl.) B*, 73:918, 1999.
- [11] J. Harada, A.S. Kronfeld, H. Matsufuru, N. Nakajima, and T. Onogi. *Phys. Rev. D*, 64:074501, 2001.

- [12] J. Harada, H. Matsufuru, T. Onogi, and A. Sugita. *Phys. Rev. D*, 66:014509, 2002.
- [13] P.B. Mackenzie, S.M. Ryan, and J.N. Simone. *Nucl. Phys. (Proc. Suppl.) B*, 63:305, 1998.
- [14] P. Chen. *Phys. Rev. D*, 64:034509, 2001.
- [15] R. Lewis, N. Mathur, and R.M. Woloshyn. *Phys. Rev. D*, 64:094509, 2001.
- [16] M. Okamoto et al. *Phys. Rev. D*, 65:094508, 2002.
- [17] A. Juettner and J. Rolf. *Phys. Lett. B*, 560:59, 2003.
- [18] Y. Nemoto, N. Nakajima, H. Matsufuru, and H. Suganuma. *Phys. Rev. D*, 68:094505, 2003.
- [19] C. Liu, J. Zhang, Y. Chen, and J.P. Ma. *Nucl. Phys. B*, 624:360, 2002.
- [20] G. Meng, C. Miao, X. Du, and C. Liu. *hep-lat/0309048*, 2003.
- [21] C. Miao, X. Du, G. Meng, and C. Liu. *hep-lat/0403028*, 2004.
- [22] X. Du, C. Miao, G. Meng, and C. Liu. *hep-lat/0404017*, 2004.
- [23] Junhua Zhang and C. Liu. *Mod. Phys. Lett. A*, 16:1841, 2001.
- [24] T. Umeda et al. *Phys. Rev. D*, 68:034503, 2003.
- [25] S. Hashimoto and M. Okamoto. *Phys. Rev. D*, 67:114503, 2003.
- [26] Justin Foley, Alan O Cais, Mike Peardon, and Sinead M. Ryan. *hep-lat/0405030*, 2004.
- [27] Junko Shigemitsu Stefan Groote. *Phys. Rev. D*, 62:014508, 2000.
- [28] H. Matsufuru, T. Onogi, and T. Umeda. *Phys. Rev. D*, 64:114503, 2001.
- [29] A. Frommer, S. Guesken, T. Lippert, B. Nöckel, and K. Schilling. *Int. J. Mod. Phys. C*, 6:627, 1995.
- [30] U. Glaessner, S. Guesken, T. Lippert, G. Ritzenhoefer, K. Schilling, and A. Frommer. *hep-lat/9605008*.
- [31] B. Jegerlehner. *hep-lat/9612014*.
- [32] X. Li and C. Liu. *Phys. Lett. B*, 587:100, 2004.
- [33] X. Feng, X. Li, and C. Liu. *Phys. Rev. D*, 70:014505, 2004.